Journal of Materials Chemistry C

Accepted Manuscript

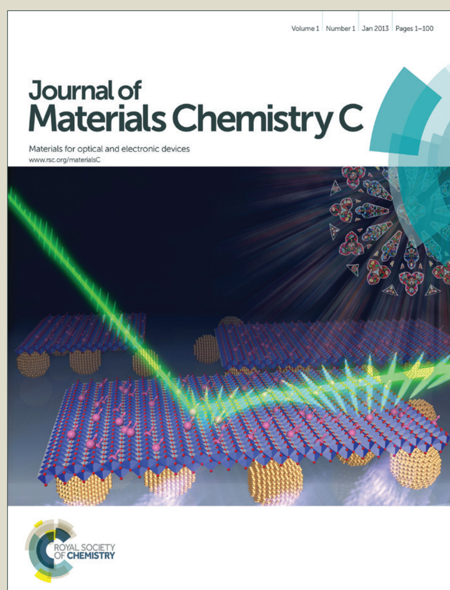

This is an *Accepted Manuscript*, which has been through the Royal Society of Chemistry peer review process and has been accepted for publication.

Accepted Manuscripts are published online shortly after acceptance, before technical editing, formatting and proof reading. Using this free service, authors can make their results available to the community, in citable form, before we publish the edited article. We will replace this *Accepted Manuscript* with the edited and formatted *Advance Article* as soon as it is available.

You can find more information about *Accepted Manuscripts* in the Information for Authors.

Please note that technical editing may introduce minor changes to the text and/or graphics, which may alter content. The journal's standard Terms & Conditions and the Ethical guidelines still apply. In no event shall the Royal Society of Chemistry be held responsible for any errors or omissions in this *Accepted Manuscript* or any consequences arising from the use of any information it contains.

ROYAL SOCIETY OF CHEMISTRY

www.rsc.org/materialsC

Journal of Materials Chemistry C RSCPublishing

ARTICLE

Cite this: DOI:

Received
Accepted

DOI:

www.rsc.org/

High density and patternable growth of silicon, germanium and alloyed SiGe nanowires by a rapid anneal protocol.

M. Bezuidenhout[1,2], T. Kennedy[2], S. Belochapkine[2], Y. Guo[2], E. Mullane[2], P.A. Kiely[1*], K.M. Ryan[2*ł]

We report the formation of silicon, germanium and alloyed $Si_{1-x}Ge_x$ nanowires by direct pyrolysis of liquid precursors on a heated substrate in an inert environment. The nanowires form in high density on the substrate with a fast reaction time. We use SEM, HRTEM, EDX-STEM, and Raman spectroscopy to carry out an in depth study into the population distribution of $Si_{1-x}Ge_x$ nanowires. The method was sufficiently adaptable to pattern the nanowire growth using standard dry film lithography techniques. Additionally, we further show that direct writing with a copper metal pen deposited sufficient catalyst to allow localised nanowire growth constrained to the treated areas.

Notes

[1] Department of Life Sciences, and Materials and Surface Science Institute, University of Limerick, Limerick, Ireland.
[2] Materials and Surface Science Institute and Department of Chemical and Environmental Sciences, University of Limerick, Limerick, Ireland.
[*] These authors contributed equally to this work
[ł] corresponding author Kevin.m.ryan@ul.ie

Introduction

Silicon and germanium nanowires (NW) are an important material set that have found significant application in photovoltaic, semiconductor, battery and biomedical devices [1-8]. The most common growth protocol for Si and Ge NWs is by vapour-liquid-solid (VLS) [9-12], or vapour-solid-solid (VSS) [13-16] mechanisms achieved using chemical vapour deposition CVD [17-19], molecular beam epitaxy (MBE) [20] or laser ablation[21]. More recently, solution based methods where NWs are nucleated and grown in supercritical fluids (SCF) [22, 23] or high boiling point solvents (HBS) have proved attractive for high density growth directly from substrates [24-30] The HBS and SCF methods also take advantage of the solvents as the carrier media for organometallic precursors in liquid form negating the requirement for silane or germane gases that are highly reactive. Recently, we developed a solvent vapour growth (SVG) system that uses the vapour zone of the HBS to achieve higher nucleation temperatures to that possible in the liquid allowing silicon nanowire production in high yield [30].

As the glass-ware setup is a batch process requiring relatively long reaction times (2 hours), the extension of the growth protocol to direct formation on a heated substrate is attractive for high throughput applications. Use of direct thermal anneal from a hot-plate has allowed formation of GeO [31] NW and vanadium oxide nanobelts [32] with a solid source in the presence of a catalyst in air [31]. Synthesis of non-oxide NWs requires an inert atmosphere and recently we showed controllable Ge NW production by pyrolysis of a HBS-precursor mix directly onto a substrate [29, 33]. In this setup, a bulk copper foil was formed into an open cylinder with the dual function of seeding the NW growth and localising the growth zone [29]. This system while dramatically reducing the growth times (hours to minutes) resulted in radial deposits of NWs of relatively low density. This approach did not work for silicon as the nucleation temperatures for copper silicide seeded Si NWs were not amenable to this method [34 29, 33].

A further requirement for many applications is the ability to pattern NW formation with abrupt terminations between features of dense growth and zero growth [35]. An array of methods to localise the NW growth by controlling the position of catalyst include: soft lithography, nanoimprint lithography, e-beam lithography and photolithography [36-39]. Masking methods using polystyrene nanospheres followed by thermal evaporation of seeding material have also been used to pattern Si NWs [40, 41] These are typically multiple step processes

Journal of Materials Chemistry C Accepted Manuscript

requiring placement of seeds and subsequent growth of nanostructures under vacuum.

Here we describe the synthesis of copper seeded Si NWs, Ge NWs, $Si_{1-x}Ge_x$ NWs and self-seeded Ge NWs in high density by rapid thermal decomposition of a liquid precursor/HBS mix directly onto a heated substrate in an inert atmosphere. Optimal growth is obtained when the vapour is confined on the substrate within a heat sink allowing higher nucleation temperatures to be homogenously obtained. The incorporation of radial fins on the confiner promotes cooling, allowing the solvent to be condensed thereby replicating the solvent vapour growth system that was successful for the batch reaction[12, 25, 42]. The system can be combined with classical lithography methods to define patterns of NWs in high density that grow in defined catalyst areas. We demonstrate that bulk materials can be used in a similar approach with a copper oxide pen that deposits sufficient catalyst to allow localised seeded NW growth of silicon or germanium NWs.

The growth of NWs without the use of a metal seed is also attractive and has been studied for various materials[43-45]. Studies carried out on self-catalysed Si NWs found that growth can be achieved in this plasma enhanced CVD system from surface roughness of a silicon wafer[46]. Here we show that direct writing with a diamond tipped pen on a silicon wafer gives sufficient surface roughness to localise non-seeded Ge NW growth. The simplicity of this process, combined with the rapid growth protocol make this attractive for a range of technological applications.

Methods

Materials characterisation

All material characterisation was carried out on as grown samples. NWs grown on substrates (Silicon wafer or stainless steel) were analysed by scanning electron microscope (SEM) Hitachi SU-70 at 5-20 kV. Transmission electron microscope (TEM) analysis was carried out by first sonicating the sample in toluene (Sigma-Aldrich ≥ anhydrous 99.8%) before being dropping onto a lacey carbon TEM grids. Analysis was conducted on a JEOL-2010 with an accelerating voltage of 200 kV equipped with energy dispersive X-ray (EDX) detector which allowed elemental analysis of individual NWs. Raman was carried out on a inVia confocal Raman spectrophotometer (Renishaw) with an optical microscope interface (Leica). Samples were exited using a 532 nm laser at room temperature, and results were recorded at 0.1% power for 30 sec.

Heatsink confiner design

The cylindrical confiner of 25 mm diameter wide by 30 mm in height was made of austenitic stainless steel 316, which is suitable for use in oxidising environments up to 870˚C [47]. To promote cooling of the cylinders internal walls 4 mm thick, circular fins of 3 mm in length 1.5 mm thick were spaced 2 mm apart along the cylinders circumference. This design allowed the 11 mm diameter × 25 mm tall reaction cavity to cool the reaction within the vessel for SVG derived NW growth. The temperature of the system was controlled by the built in PID in the Stuart hotplate microcontroller, and was cross referenced using an infrared gun (Heatsink confiner design in supplementary Figure S1.)

Mask preparation and thermal evaporation

Simple mask preparations were performed using a dry film photoresist, in which a polyolefin separator sheet was removed from the photoresist film before placing onto the substrate. The substrate, either stainless steel or silicon wafer, and the film were then passed through a laminator before the printed mask was applied to the surface of the film. Samples were then placed under a 45 W UV bulb at a 15 cm head height for 3-5 min before being stored in the dark for 10 min to allow polymerisation. They were then placed in 40 mM $NaHCO_3$ solution for 3 min with light agitation. Samples were then placed into a MB-EcoVap Mbraun integrated thermal evaporator where a coating of 1-10 nm of copper was applied to the substrates. Samples were then removed and soaked in acetone for 10 min to remove the dry film photoresist.

Copper oxide pen preparation

Thin copper bars were fashioned into a sharp pen before being soaked in 50 mM nitric acid for 30 min to remove any surface oxide. Pens were then removed and placed in toluene before drying. Dry pens were placed on a hotplate at 400˚C in ambient air for 10 min to form a thick oxide and then cooled to room temperature before use. Desired patterns were then written onto the substrate. All substrates were cleaned before mask preparation in acetone under sonication and then toluene before being plasma cleaned for 5 min.

Synthesis of $Si_{1-x}Ge_x$ nanowires

Substrates (Silicon wafer or stainless steel) were then placed into a MB-EcoVap Mbraun integrated thermal evaporator where a coating of 1-10 nm of copper was applied. The substrates were then placed into a designated SVG confiner and heated to 460˚C before injecting a mixed solution. The solution was made up by first mixing phenylsilane (Sigma Aldrich 97%) and diphenylgermane (DPG) (>95% Gelest) in varying concentrations (0.1-0.4% V/V DPG/PS). The solution mix was then added to Squalane (Sigma Aldrich 99%) in a 3:1 ratio respectively. Injections of 15 μL were administrated every 15 min over a 45 min reaction. The confiner was then removed and allowed to cool to room temperature. At this stage, the reaction was considered finished and the substrate were stored in toluene over night as good practice to remove any loose NWs or impurities before analysis (this procedure was followed for all the following syntheses).

Synthesis of silicon nanowires

A silicon wafer which would act as the substrate was prepared by placing it into a MB-EcoVap Mbraun integrated thermal evaporator where a coating of 1-10 nm of copper was applied onto the surface. The substrates were then placed into the silicon NW designated SVG confiner and heated to 460˚C before injecting phenylsilane (PS) (Sigma Aldrich 97%) with Squalane (Sigma Aldrich 99%) 3:1 respectively. Injections of 15 μL were administrated every 15 min over a 45 min reaction.

Journal of Materials Chemistry C Accepted Manuscript

 This journal is © The Royal Society of Chemistry 2015

The confiner was then removed and allowed to cool to room temperature. .

Synthesis of germanium nanowires

The substrate (Si wafer or stainless steel) was treated by placing it into a MB-EcoVap Mbraun integrated thermal evaporator where a coating of 1-10 nm of copper was applied or via the oxide pen or dry film photoresist methods above. The silicon/ stainless steel substrates were then placed into the SVG confiner and heated to 430˚C before injecting Diphenylgermane (DPG) (>95% Gelest) with Squalane (Sigma Aldrich 99%) 3:1 respectively. A single injection of 15µL was delivered over a 1-10 min reaction. The confiner was then removed and allowed to cool to room temperature.

Self-seeded germanium nanowires

A silicon wafer which would act as the substrate was scratched with a diamond scribe on the smooth surface. The substrates were then cleaned thoroughly with toluene to remove any debris content that resided. Samples were then placed into self-seeded germanium designated SVG confiner and heated to 430˚C before injecting Diphenylgermane (DPG) (>95% Gelest) with Squalane (Sigma Aldrich 99%) 3:1 respectively. A single injection of 15 µL was delivered over a 5-10 min reaction. The confiner was then removed and allowed to cool to room temperature.

Results and discussion

Setup overview

The general synthetic protocol is outlined in Figure 1A. In this system, the heat sink maximises thermal decomposition of the precursors whereas the cooling fins, cool the walls of the confiner allowing the reflux of the solvent vapour to maximise the residence time and improve yield in this open system. Ge NWs were grown from a thermally evaporated copper layer on a stainless steel substrate using the heatsink confiner at 430˚C allowing high density NW growth in a 2 min reaction as shown in SEM image (Figure 1B inset). The NWs establish a dense network with individual NWs showing a high degree of tortuosity due to defect driven directional growth changes that have been previously established in this system[25, 48] (Figure 1B). As the reaction conditions at 430˚C are below the eutectic point of copper and germanium, NW growth occurs by a vapour-solid-solid (VSS) mechanism. At very high density, the Ge NWs form into NW-mats ~ 10 µm thick, that cleave from the substrate (Highlighted by a white arrow) (Figure 1C). A tilted SEM image of the cross section of these NW mats, shows a dense self-supporting network of both torturous and straight NWs (Figure 1D). Interestingly, the NW mat network seems to consist of two distinct layers, the bottom predominantly occupied by tortuous larger diameter Ge NWs and the top composed of highly intertwined thinner diameter Ge NWs. The torturous NWs range from 70-120 nm in diameter whereas the straight NWs typically range from 20-30 nm. HRTEM of the straight NW of 30nm diameter growing in the <110> direction is seen in figure 1E, possessing stacking faults that run parallel to the NW axis. The Cu seed at the tip of the Ge NW, is evident by its higher z-contrast, and can be indexed to Cu_3Ge by electron diffraction (inset top Figure 1E) with the NW body indexing to diamond cubic germanium as expected (inset bottom Figure 1E). The elemental composition was further supported by Energy-dispersive X-ray spectroscopy (EDX) of the high angle annular dark field (HAADF)-STEM Ge NW (inset Figure 1F). An elemental line scan of the NW indicated by the white line is graphed in figure 1F showing the presence of a copper seed and germanium NW body. XRD of the Ge NWs confirm the diamond cubic germanium phase (Supplementary Figure S2). Interestingly, the NWs can also be produced in oxygen rich environments within fume hoods with a small volume of precursor and show minimal difference in NW morphologies compared to that produced under inert conditions. However, scaling this approach to large volume is not practical due to safety risks (Supplementary Figure S3).

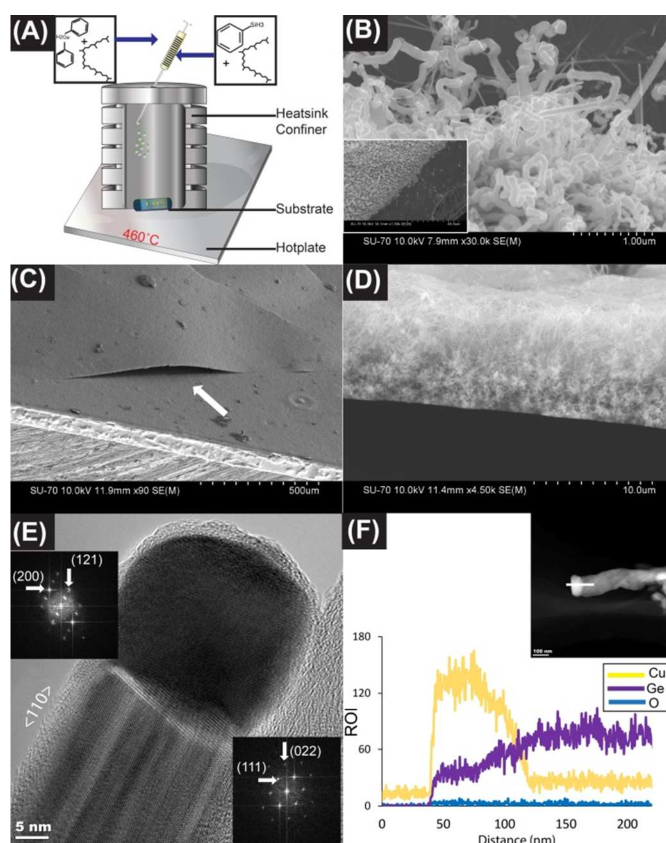

Figure 1: Germanium Nanowire material characteristics. (A) Reaction setup using heatsink confiner hotplate method. (B) High magnification SEM image of Ge NWs with inset a tilted image of Ge NWs in high density on the substrate. (C) Tilt SEM image of Ge NW-Mat peeling away from the stainless steel substrate. (D) An SEM image viewing the cross-section of a NW mat. (E) HRTEM of a Ge NW with a <110> growth direction growing from a copper germanide seed with FFT inset. (F) EDX line profile analysis of inset HAADF-STEM showing Ge NW with Cu seed.

Copper silicide seeded silicon wires

Journal of Materials Chemistry C Accepted Manuscript

Extension of NW growth to silicon is challenging as the decomposition of the phenylsilane must be carried out at reaction temperatures of 460˚C or higher to facilitate the phenyl redistribution chemistry that provides the in-situ silicon source for NW growth [34]. This has not been possible previously using a hot-plate approach as it is difficult to regulate the temperature and the solvent-vapour dwell time. Here using the heat sink confiner, Si NWs figure 2A were successfully grown in high density (revealed by a yellow colour) from a thermally evaporated copper layer on a silicon wafer substrate at 460˚C (Figure 2A and inset). Again, the growth mechanism is VSS, as the reaction temperature is carried out far below the eutectic point of copper and silicon. A tilted SEM image of the Si NWs show that even beneath the dense growth some seeds remain un-reacted allowing for further densification to occur with subsequent monomer injections (Figure 2B). A HRTEM image of a single Si NW (75 nm in diameter) shows clear stacking faults along the NW axis growing in a <111> direction with the darker Cu seed evident at the tip of the NW from its higher Z-contrast (Figure 2C). SAED of the Si NW was found to index to cubic silicon and was supported by XRD for a large sample (Figure 2C inset; Supplementary Figure S4). EDX elemental analysis in figure 2D shows the line scan results from the white line in the HAADF-STEM image inset. This confirms the silicon and metal rich regions respectively. These high density NWs have applications in lithium ion batteries as anode materials [49] (supplementary figure S7).

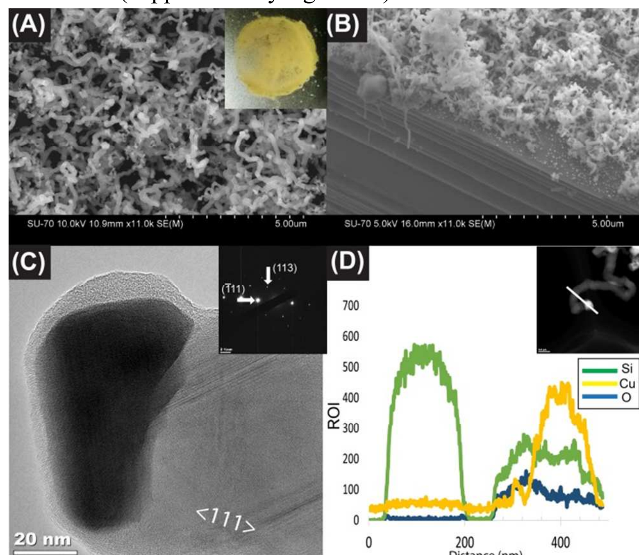

Figure 2: Silicon Nanowire material characteristics. (A) SEM image of nanowires with inset photo of product after reaction. (B) Tilt SEM image cross section showing unreacted seeds. (C) HRTEM analysis of a Si NW showing the copper silicide seed in darker contrast. The inset is of SAED pattern of Si NW is indexed to cubic silicon. (D) EDX line profile analysis of inset dark field STEM showing Si NW with copper silicide seed.

Alloyed SiGe nanowire

The control within the setup can be extended to the formation of alloyed materials where mixing DPG and PS (0.4% V/V) can produce $Si_{1-x}Ge_x$ NWs. The $Si_{1-x}Ge_x$ NWs were grown in high density (Figure 3A) from a thermally evaporated Cu layer (~10 nm). The network comprises a bimodal distribution with larger diameter tortuous NWs labelled (i) and thinner diameter straight NWs (ii) figure 3B. Interestingly this co-occurrence of larger and narrower diameter NW is also observed in the seeded Ge NWs but is not seen in the pure Si NWs. The NW size is governed by the seed size and here the agglomeration of the thermally evaporated copper layer during heating into distinct copper islands provide the seeds for the NW growth in agreement with other works[50-52]. The data is portrayed in figure 3C, were we observe an increase in the copper island particle size with increasing temperature and anneal time (an SEM image of the initial evaporated layer is shown in supplementary figure S5). A plot of the copper island particle size distribution frequency is shown for each condition of temperature and anneal time (Figure 3D). The expected trend towards larger agglomerated particles with increased temperature and anneal time is evident. Noticeably the lower temperature associated with the conditions suitable for Ge NW growth and shorter times also give rise to smaller copper islands 30-40 nm in diameter in agreement with observed smaller NWs.

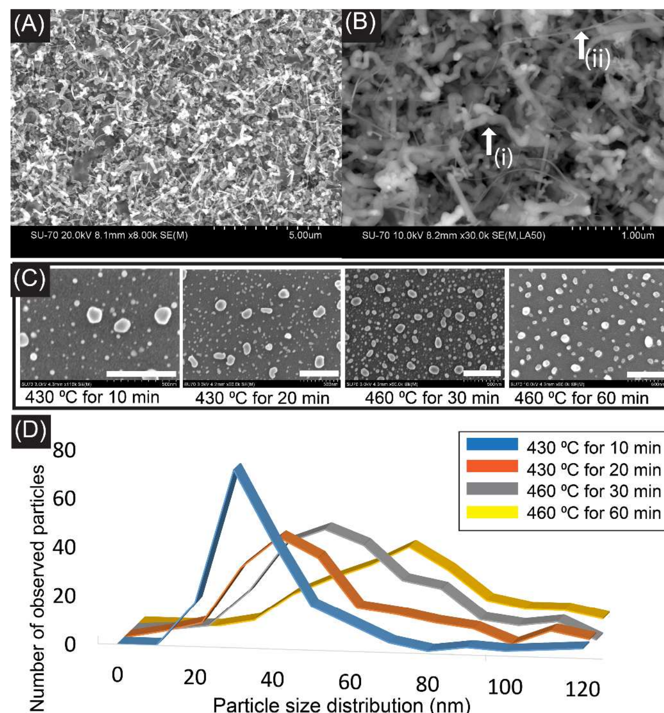

Figure 3: $Si_{1-x}Ge_x$ Nanowire material characteristics. (A) SEM image of high density $Si_{1-x}Ge_x$ NWs. (B) SEM image showing individual $Si_{1-x}Ge_x$ NWs on substrate surface with bimodal NW distribution. The white arrow (i) highlights a typical larger diameter NW were as (ii) highlights a typical smaller diameter NW. (C) A series of SEM images showing the effect of increased temperature and reaction temperature on the coalescence of a thermally evaporated copper layer, the white bar in all images is representative of 500 nm. (D) A frequency population distribution plot of the conditions seen in C above. With increasing time and temperature there is a tendency to larger copper islands.

Journal of Materials Chemistry C Accepted Manuscript

This journal is © The Royal Society of Chemistry 2015

Closer inspection of the alloyed NWs show that both <111>, and <110> growth directions are present. Figure 4A shows a typical TEM image of a smaller $Si_{1-x}Ge_x$ NW of 35nm with a <110> growth direction (as confirmed by SAED inset top Figure 4A). HRTEM of the $Si_{1-x}Ge_x$ NW edge (bottom inset Figure 4A), shows an amorphous oxide coating of 3-5 nm. By tilting the larger $Si_{1-x}Ge_x$ NW in figure 4B along a kikuchi pattern line by 35.5° between two zone axes we were able to confirm its cubic phase. The diffraction patterns for this material can be indexed to a cubic Si-Ge alloy, when viewed down the <11-1> beam direction (Figure 4B top inset), and when tilted to view down the <01-1> beam direction (Figure 4B bottom inset). Slight deviations in the lattice parameter from Vegard's law are observed and agree with related works[53].

The elemental composition of the $Si_{1-x}Ge_x$ NWs seen in figure 4B was evaluated using an EDX line scan (Figure 4C), the scan path is highlighted in figure 4B with a solid white line from left to right. The line scan for the larger NW (85 nm diameter) shows a richer silicon composition, when compared to germanium. The thinner NW (30 nm diameter) is shown to have more equivalent amounts of silicon and germanium present in its distribution. To investigate whether this trend was conserved across the population a Welch t-test was performed, using a multipoint EDX analysis along the length of the $Si_{1-x}Ge_x$ NWs. The sample size was N≥10 NWs for each diameter population large (70-120 nm) and thin (30-50 nm). The data is presented as a bar chart below of the relative atomic percentage between silicon and germanium (Figure 4D), with error bars of 1 standard deviation in each direction. The 70-120 nm diameter NWs have a distinct consistency within the population with statistically more silicon than germanium. However, the distribution of silicon and germanium in the 30-50 nm diameter NWs is not consistent (Figure 4D). In this study of 0.4% Ge v/v (DPG/PS) at 460°C for 45 min, the germanium for the larger $Si_{1-x}Ge_x$ NWs was found to be (Ge) x=0.22 producing a tightly disperse population of $Si_{0.78}Ge_{0.22}$. However, the smaller NWs were found to have a mean (Ge) x=0.35 giving a mean population of $Si_{0.65}Ge0_{.35}$.

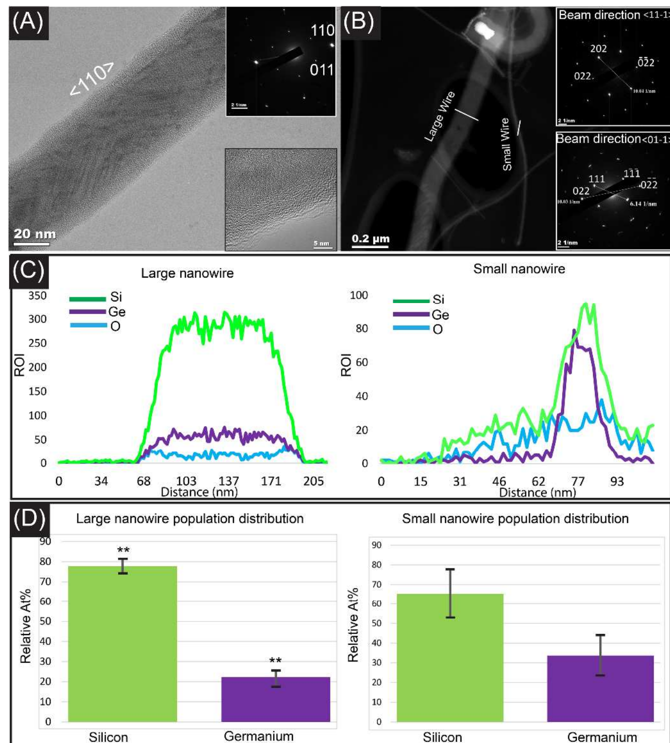

Figure 4: $Si_{1-x}Ge_x$ NW population elemental characteristics. (A) TEM image of a 35 nm diameter $Si_{1-x}Ge_x$ NW (0.4% V/V). Inset top shows an indexed SAED of the $Si_{1-x}Ge_x$ NW, and 2D fringing of the $Si_{1-x}Ge_x$ NW is seen in the bottom inset. (B) Dark field STEM of $Si_{1-x}Ge_x$ NWs, Inset top showing SAED of the larger diameter NW indexed for cubic Si:Ge alloy along the beam direction <11-1>, and inset bottom along the beam direction <01-1> after tilting 35.5°.(C) EDX line profile analysis of figure B dark field STEM, showing the large NW and the thin NW respectively. (D) Population study of large (70-120 nm) NWs and small (30-50 nm) NWs Ge:Si distribution N≥10 NWs for each diameter population.

An EDX elemental map of a large $Si_{1-x}Ge_x$ NW (70 nm diameter) shows a continual distribution of silicon and germanium throughout the NW, re-enforcing the evidence of an alloyed NW (Figure 5A). XRD of the $Si_{1-x}Ge_x$ NWs confirms the cubic phase of the alloy with interesting peak splitting possibly due to the mixed sample containing both smaller diameter and large diameter NWs with different distribution of Si:Ge ratio (Supplementary Figure S6).

In order to further study the effect of varying concentration of the Ge component in the reaction, a study of three concentrations 0.4%V/V, 0.25%V/V, and 0.1%V/V (DPG/PS) was used in a Raman study of the alloy component. The presence of alloy NW composition in the sample was determined by Raman. Three predominate bands were found when examining hundreds of NWs in random orientations relative to the incident polarization at room temperature. They were the Ge-Ge band (294-299cm^{-1}), Si-Ge band (400-402cm^{-1}) and Si-Si band (513-518cm^{-1}) [54] (Figure 5B). Shifts in the band position relative to the pure NW materials is due to the alloy composition of the NWs. We observed that decreasing the concentration towards 0.1% V/V (DPG/PS) resulted in a lower

Journal of Materials Chemistry C Accepted Manuscript

intensity Si-Ge peak, whereas increasing the concentration of the Ge precursor in the reaction mix resulted in relatively higher intensity alloy peak. We found that exceeding 0.4% V/V (DPG/PS) resulted in a mixture of alloy NWs and pure germanium NWs as determined by EDX.

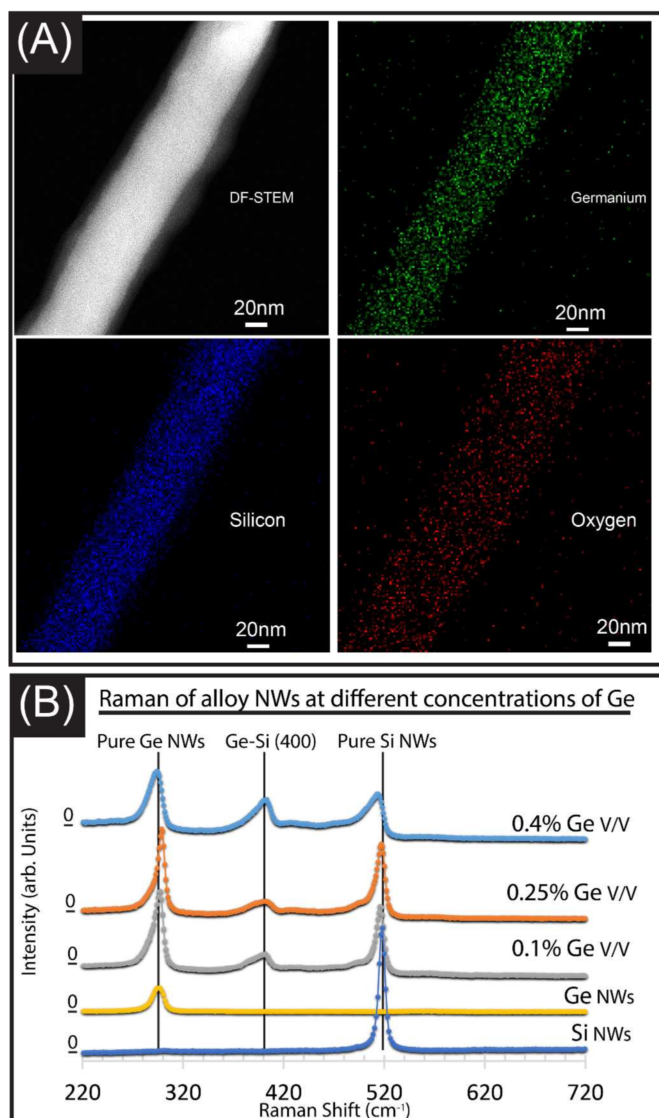

Figure 5: $Si_{1-x}Ge_x$ Nanowire elemental characteristics. (A) EDX Elemental mapping of the large NW showing the dispersion of Oxygen, Germanium, and silicon throughout the NW. (B) Raman of $Si_{1-x}Ge_x$NWs grown on a stainless steel substrate. A batch of samples were produced under the given reaction conditions 0.1, 0.25, 0.4% V/V DPG and shown with three predominate bands observed at (294-299cm^{-1}) for Ge-Ge in a silicon environment, (400-402 cm^{-1}) for Ge-Si band, and (513-518 cm^{-1}) for the Si-Si band in a germanium rich environment.

Localised patterning of NW using the heatsink confiner

Having demonstrated the variety of nanomaterials that the heatsink method is capable of producing at high densities, we sought to impart patterning control of the NWs directly from the substrate using a number of techniques. Firstly, patterning control was performed using a classical dry film photoresist lithography technique, in combination with a thermally evaporated copper layer onto a silicon wafer, to produce both Ge NWs and Si NWs. A mask of letters "UL" was used to designate the patterning of the NWs on the silicon substrate. Figure 6A shows a tilt SEM images of the substrates after Ge NWs growth showing the high localised density of the nanomaterial. The letters "UL" (inset Figure 6A) are visible at low magnification were the NW growth is visible through the contrast difference. A closer examination of the boundary (Figure 6B) highlighted as a white box in figure 6A shows a mixture of larger diameter tortuous NWs and smaller diameter straighter NWs spanning into the unseeded areas along the boundary.

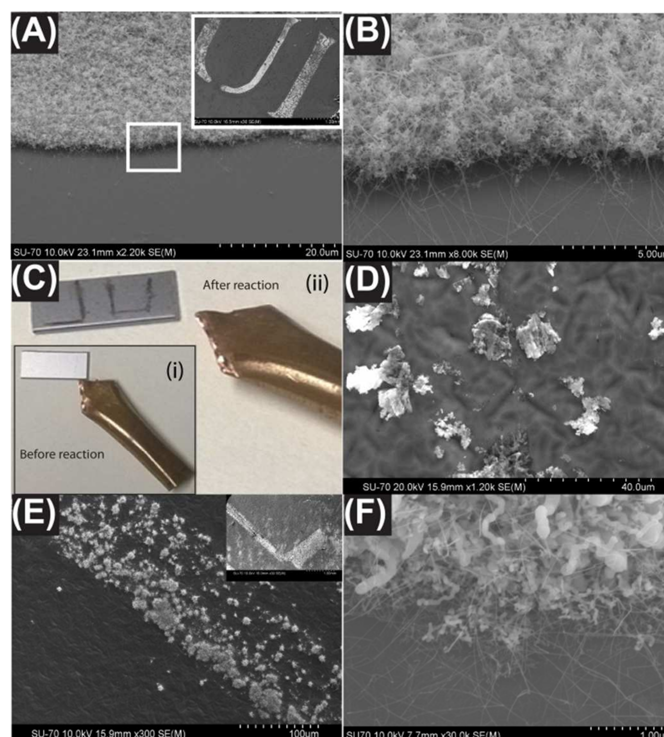

Figure 6: Patterning Dense growth of Ge NWs using Dry film lithography. (A) A SEM image of Ge NWs grown on a silicon wafer substrate in high density within the patterned area of the letters "UL" seen in the inset top right. (B) A closer SEM image of the pattern boundary between the Ge NWs growth area and the silicon substrate seen within the white box. (C) A copper oxide pen, with the letters "UL" written onto a silicon before the reaction (i) and after the reaction (ii). (D) Seeding material deposited onto a silicon wafer by the copper oxide pen before a reaction. (E) A tilted SEM image of the pattern boundary produced in a Ge NW reaction. The letter "L" seen in the inset of a low magnification SEM image donating the location of NW growth. (F) A high resolution SEM image of the NWs produced with copper oxide flakes as seeding material.

Conventional lithography is a multi-step process. However, for many applications (covert security features etc.), the ability to directly write patterns is advantageous. By taking a piece of bulk copper foil fashioned into a pen and subjecting it to a mild oxidation we were able to write on the surface of a

Journal of Materials Chemistry C Accepted Manuscript

This journal is © The Royal Society of Chemistry 2015

wafer and thereby deposit sufficient catalyst to achieve patterned growth. Figure 6C (i) shows a copper oxide pen where the letters “UL” were scribed onto the surface of a silicon wafer before a reaction, the abrasion of the copper oxide pen surface on the silicon was sufficient to leave thin flakes of copper oxide behind as seeding material. Figure 6C (ii) shows the wafer after reaction were the copper oxide flakes have reacted in a germanium reaction setup to produce localised dense fields of Ge NWs. The copper oxide flakes deposited on the surface of the silicon wafer are seen in figure 6D, the typical deposit flakes can range from 0.5-15 µm in length which appears to be sufficient to seed localised dense NWs. Closer inspection (Figure 6E) of the dense growth seen in figure 6C (ii) shows dense localised growth along a line with island like growth possibly due to the areas of flake deposition during abrasion. A low magnification SEM image of the letter “L” is seen in figure 6E-inset, showing the brighter contrast areas of NW growth compared to the darker silicon substrate. High resolution SEM of the NWs produced in these areas show a mixture of larger diameter tortuous NWs, and thinner diameter straight NWs (Figure 6F). Although data for only germanium was shown here this method works for both the alloys and Si NWs.

Self-seeded germanium nanowires

Self-seeded Ge NWs have been obtained previously in the solvent vapour growth system. While there is debate as to the source of nucleation in these materials, one particular relevant theory is that the HBS organic droplets act in the same way as the metal catalyst, were the absorption of Ge is mediated not by the solubility but rather the low diffusion resistance of small droplets[55, 56]. Some suggestion indicate that the breakdown of the organometallic precursors can result in alkyl radicals which themselves are capable of further decomposition of the original precursor [57] or the presence of a phenyl group was necessary in the growth of the NWs[58]. The extent of growth of self-seeded NWs within the system were found to amplify by increasing the surface area of the substrate by roughness.

Here using a diamond scribe to produce a rougher surface on a smooth silicon wafer we are able to achieve this localised high density growth of Ge NWs without deliberate seeding using a DPG/HBS solution. The self-seeded Ge NWs produce a defined pattern boundary (Figure 7A), along the scribed letter “L” seen in the low magnification SEM image (Figure 7A Inset). Closer inspection of the boundary within the indicated white box in figure 7A shows individual Ge NWs with diameters of 15-30 nm without seeds at their tips (Figure 7B). In order to achieve localised growth by this system, the substrate needs to be clean of any impurities or dust, as NW growth will occur in those areas. The reaction is time sensitive, a prolonged reaction will result in full substrate coverage and the ability to readily remove the precursor and prevent overgrowth is a distinct advantage. The mechanism of the increased growth in rougher areas is not clear. Any number of factors, such as: (i) a higher availability of surface area, to grow from may result in a faster rate of NW formation leading to denser growth. (ii) The organic vapour may reside longer in the rough areas of the substrate compared to smoother areas of the substrate. (iii) The boundary layer of gaseous movement over the rougher surface lends itself to more turbulent mixing of vapour increasing the possibility of NW nucleation. HRTEM of a single Ge NW of 23 nm diameter shows a high degree of crystallinity visible as fringes along the NW (Figure 7C). FFT of the single crystal NW can be indexed to diamond cubic germanium (Figure 7C inset). In EDX analysis and HAADF-STEM no evidence of discrete catalyst particles were apparent (Figure 7D inset). An elemental line scan across the NWs shown by the white line (Figure 7D), shows the presence of germanium and oxygen in agreement with the above observed data.

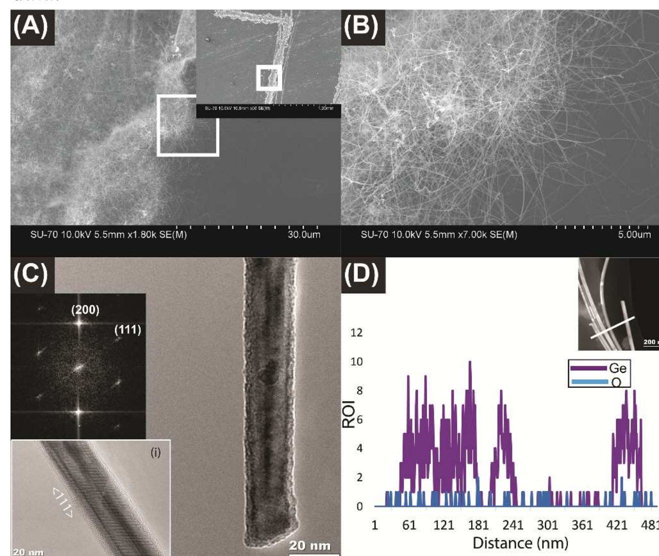

Figure 7: Patterning Self-Seeded Germanium Nanowire. (A) SEM image of Ge NWs patterned using a diamond scribe roughened silicon wafer surface. Inset shows a low magnification SEM image of the letter “L”, Ge NWs produce a lighter contrast on the scribed wafer. (B) A closer SEM image of (A) showing the pattern boundary within the white box between the Ge NWs growth area and the substrate. (C) TEM image of a Ge NW showing crystalline fringes. Inset a FFT of the Ge NWs indexed to diamond cubic germanium from the HRTEM image inset below (i). (D) EDX line profile analysis of inset HAADF-STEM showing self-seeded germanium NW.

Conclusion

In this report we present a generally applicable protocol for the rapid production of: Ge, Si, $Si_{1-x}Ge_x$ and Self-seeded Ge NWs on silicon and stainless steel substrates. The system comprises a heated substrate with a growth zone confined by a heat sink contained in an inert atmosphere. The system is sufficiently adaptable to allow patterned growth with conventional lithography or patterning of locations defined by simply drawing with a metal pen directly onto substrates. The additional patterning control of Self-seeded Ge NWs on the substrate by creating rough areas using a diamond scribe was also demonstrated.

Journal of Materials Chemistry C Accepted Manuscript

References

1. B. Tian, T. J. Kempa and C. M. Lieber, *Chemical Society Reviews*, 2009, **38**, 16-24.
2. Q. Qing, Z. Jiang, L. Xu, R. Gao, L. Mai and C. M. Lieber, *Nature Nanotechnology*, 2013, **9**, 5.
3. C. K. Chan, X. F. Zhang and Y. Cui, *Nano Letters*, 2007, **8**, 307-309.
4. T. Kennedy, E. Mullane, H. Geaney, M. Osiak, C. O'Dwyer and K. M. Ryan, *Nano Letters*, 2014, **14**, 716-723.
5. Y. Cui, Z. Zhong, D. Wang, W. U. Wang and C. M. Lieber, *Nano Letters*, 2003, **3**, 149-152.
6. A. B. Greytak, L. J. Lauhon, M. S. Gudiksen and C. M. Lieber, *Applied Physics Letters*, 2004, **84**, 4176-4178.
7. J.-S. Huang, C.-Y. Hsiao, S.-J. Syu, J.-J. Chao and C.-F. Lin, *Solar Energy Materials and Solar Cells*, 2009, **93**, 621-624.
8. M. Bezuidenhout, P. Liu, S. Singh, M. Kiely, K. M. Ryan and P. A. Kiely, *PloS one*, 2014, **9**, e108006.
9. R. S. Wagner and W. C. Ellis, *Applied Physics Letters*, 1964, **4**, 89-90.
10. Y. Cui, L. J. Lauhon, M. S. Gudiksen, J. Wang and C. M. Lieber, *Applied Physics Letters*, 2001, **78**, 2214-2216.
11. X. Lu, T. Hanrath, K. P. Johnston and B. A. Korgel, *Nano Letters*, 2002, **3**, 93-99.
12. H. Geaney, T. Kennedy, C. Dickinson, E. Mullane, A. Singh, F. Laffir and K. M. Ryan, *Chemistry of Materials*, 2012, **24**, 2204-2210.
13. J. Arbiol, B. Kalache, P. R. i Cabarrocas, J. R. Morante and A. F. i Morral, *Nanotechnology*, 2007, **18**, 305606.
14. Y. Yao and S. Fan, *Materials Letters*, 2007, **61**, 177-181.
15. Y. Wan, Z. Wang, Y. Fang, Z. Xia, Y. Wang and J. Sha, *Materials Letters*, 2010, **64**, 1839-1842.
16. F.-W. Yuan, C.-Y. Wang, G.-A. Li, S.-H. Chang, L.-W. Chu, L.-J. Chen and H.-Y. Tuan, *Nanoscale*, 2013, **5**, 9875-9881.
17. Y. Wu and P. Yang, *Chemistry of Materials*, 2000, **12**, 605-607.
18. V. Schmidt, J. V. Wittemann and U. Gösele, *Chemical Reviews*, 2010, **110**, 361-388.
19. S. V. Thombare, A. F. Marshall and P. C. McIntyre, *Journal of Applied Physics*, 2012, **112**, 054325.
20. L. Schubert, P. Werner, N. Zakharov, G. Gerth, F. Kolb, L. Long, U. Gösele and T. Tan, *Applied Physics Letters*, 2004, **84**, 4968-4970.
21. A. M. Morales and C. M. Lieber, *Science*, 1998, **279**, 208-211.
22. J. D. Holmes, K. P. Johnston, R. C. Doty and B. A. Korgel, *Science*, 2000, **287**, 1471-1473.
23. O. Lotty, R. Hobbs, C. O'Regan, J. Hlina, C. Marschner, C. O'Dwyer, N. Petkov and J. D. Holmes, *Chemistry of Materials*, 2013, **25**, 215-222.
24. C. A. Barrett, H. Geaney, R. D. Gunning, F. R. Laffir and K. M. Ryan, *Chemical Communications*, 2011, **47**, 3843-3845.
25. H. Geaney, C. Dickinson, C. A. Barrett and K. M. Ryan, *Chemistry of Materials*, 2011, **23**, 4838-4843.
26. H. Geaney, C. Dickinson, W. Weng, C. J. Kiely, C. A. Barrett, R. D. Gunning and K. M. Ryan, *Crystal Growth & Design*, 2011, **11**, 3266-3272.
27. A. T. Heitsch, C. M. Hessel, V. A. Akhavan and B. A. Korgel, *Nano Letters*, 2009, **9**, 3042-3047.
28. A. M. Chockla and B. A. Korgel, *Journal of Materials Chemistry*, 2009, **19**, 996-1001.
29. E. Mullane, H. Geaney and K. M. Ryan, *Chemical Communications*, 2012, **48**, 5446-5448.
30. H. Geaney, E. Mullane and K. M. Ryan, *Journal of Materials Chemistry C*, 2013, **1**, 4996-5007.
31. M. Farhan, M. A. Khan and T. P. Hogan, *Journal of Alloys and Compounds*, 2010, **508**, L21-L23.
32. Y. Zhu, Y. Zhang, L. Dai, F.-C. Cheong, V. Tan, C.-H. Sow and C.-T. Lim, *Acta Materialia*, 2010, **58**, 415-420.
33. E. Mullane, T. Kennedy, H. Geaney and K. M. Ryan, *ACS Applied Materials & Interfaces*, 2014, **6**, 18800-18807.
34. H.-Y. Tuan and B. A. Korgel, *Chemistry of Materials*, 2008, **20**, 1239-1241.
35. G. Yu and C. M. Lieber, *Pure and Applied Chemistry*, 2010, **82**, 2295-2314.
36. Z. Fan, J. C. Ho, Z. A. Jacobson, R. Yerushalmi, R. L. Alley, H. Razavi and A. Javey, *Nano Letters*, 2007, **8**, 20-25.
37. T. Mårtensson, P. Carlberg, M. Borgström, L. Montelius, W. Seifert and L. Samuelson, *Nano Letters*, 2004, **4**, 699-702.
38. D. Whang, S. Jin, Y. Wu and C. M. Lieber, *Nano Letters*, 2003, **3**, 1255-1259.
39. F. Li, M. Zhu, C. Liu, W. L. Zhou and J. B. Wiley, *Journal of the American Chemical Society*, 2006, **128**, 13342-13343.
40. B. Fuhrmann, H. S. Leipner, H.-R. Hoeche, L. Schubert, P. Werner and U. Gösele, *Nano letters*, 2005, **5**, 2524-2527.
41. J. C. Hulteen and R. P. Van Duyne, *Journal of Vacuum Science & Technology A*, 1995, **13**, 1553-1558.
42. C. A. Barrett, H. Geaney, R. D. Gunning, F. R. Laffir and K. M. Ryan, *Chemical Communications*, 2011, **47**.
43. R. P. Sugavaneshwar and K. K. Nanda, *Scientific Reports*, 2013, **3**, 1172.
44. S. Mathur, H. Shen, V. Sivakov and U. Werner, *Chemistry of Materials*, 2004, **16**, 2449-2456.
45. V. Dřínek, R. Fajgar, M. Klementova and J. Šubrt, *Journal of The Electrochemical Society*, 2010, **157**, K218-K222.
46. M. Cuscunà, A. Convertino, L. Mariucci, G. Fortunato, L. Felisari, G. Nicotra, C. Spinella, A. Pecora and F. Martelli, *Nanotechnology*, 2010, **21**, 255601.
47. M. Handbook, *Materials Park, OH*, 1990, **2**, 152-177.
48. K. Kang, G. H. Gu, D. A. Kim, C. G. Park and M.-H. Jo, *Chemistry of Materials*, 2008, **20**, 6577-6579.
49. Tadhg Kennedy, Michael Bezuidenhout, Kumaranand Palaniappan, Killian Stokes, Michael Brandon and K. M. Ryan, *ACS Nano*.
50. D. Srolovitz and M. Goldiner, *JOM*, 1995, **47**, 31-36.
51. J.-Y. Kwon, T.-S. Yoon, K.-B. Kim and S.-H. Min, *Journal of Applied Physics*, 2003, **93**, 3270-3278.
52. R. Saxena, W. Cho, O. Rodriguez, W. N. Gill and J. L. Plawsky, *Journal of Non-Crystalline Solids*, 2004, **350**, 14-22.
53. E. Kasper, A. Schuh, G. Bauer, B. Holländer and H. Kibbel, *Journal of crystal growth*, 1995, **157**, 68-72.
54. Q. Lu, K. W. Adu, H. R. Gutiérrez, G. Chen, K.-K. Lew, P. Nimmatoori, X. Zhang, E. C. Dickey, J. M. Redwing and P. C. Eklund, *The Journal of Physical Chemistry C*, 2008, **112**, 3209-3215.
55. N. Zaitseva, J. Harper, D. Gerion and C. Saw, *Applied Physics Letters*, 2005, **86**, 053105.
56. A. A. Chernov, *Modern crystallography*, Springer, 1984.
57. H. S. Taylor and W. H. Jones, *Journal of the American Chemical Society*, 1930, **52**, 1111-1121.
58. J. R. Heath and F. K. LeGoues, *Chemical Physics Letters*, 1993, **208**, 263-268.

Acknowledgements

We are grateful to our colleagues in the laboratory of nanotechnology for helpful discussions and critical review as well as to members of MSSI group especially Dr. Lekshmi Kailas for her help on the Raman alloy nanowires samples.

Funding bodies

This work was supported in whole by grants received from the Irish Research Council Postgraduate Scholarship Scheme (MB) and by Science Foundation Ireland (SFI) under the Principal Investigator Program (Contract No. 11PI-1148) (KMR), and SFI's CDA program (13/CDA/2228) (PAK), and was conducted under the framework of the Irish Government's Programme for Research in Third Level Institutions Cycle 5, National Development Plan 2007–2013 with the assistance of the European Regional Development Fund (KMR).

Journal of Materials Chemistry C Accepted Manuscript

 This journal is © The Royal Society of Chemistry 2015

Journal of Materials Chemistry C Accepted Manuscript

This journal is © The Royal Society of Chemistry 2015

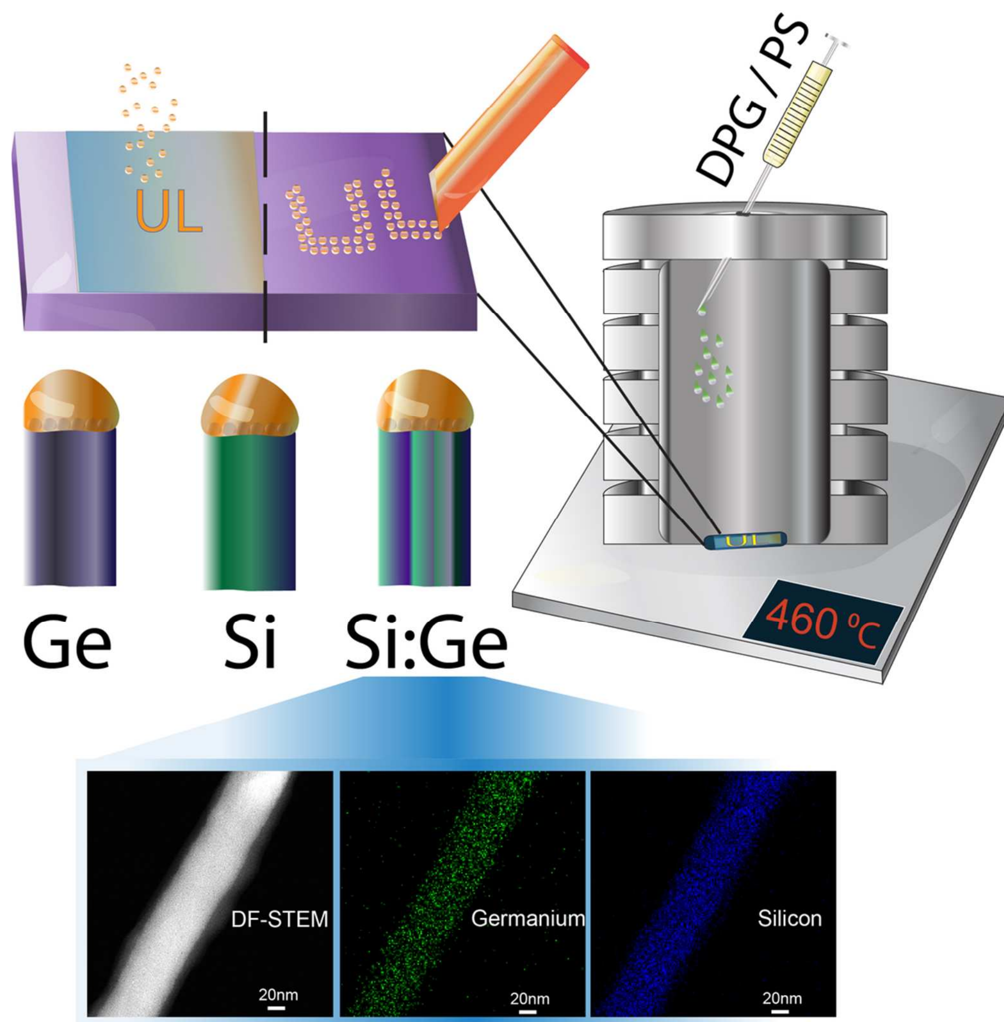

We report the formation of silicon, germanium and alloyed Si1-xGex nanowires by direct pyrolysis of liquid precursors on a heated substrate in an inert environment. The nanowires form in high density on the substrate with a fast reaction time. We use SEM, HRTEM, EDX-STEM, and Raman spectroscopy to carry out an in depth study into the population distribution of Si1-xGex nanowires. The method was sufficiently adaptable to pattern the nanowire growth using standard dry film lithography techniques. Additionally, we further show that direct writing with a copper metal pen deposited sufficient catalyst to allow localised nanowire growth constrained to the treated areas.
98x100mm (300 x 300 DPI)

Journal of Materials Chemistry C Accepted Manuscript